Structural Investigations of Solid Proteins at Natural Abundance Using 2D Multiple-Pulse NMR

Jeffery L. White* and Xingwu Wang

Department of Chemistry, North Carolina State University, Campus Box 8204, Raleigh, North Carolina 27695-8204

Received November 27, 2001

ABSTRACT: Results from multiple-pulse 2D $^1H-^{13}C$ correlation experiments are described for natural proteins in the solid state. Detailed HETCOR experiments on the complex silk fibroin proteins *Samia cynthia ricini (S. c. ricini)* and *Bombyx mori (B. mori)* demonstrate that while the expected dipolar-mediated ^{13}C and ^1H correlations are observed, additional chemical shift and coupling information involving amide linkages and dilute peptides are also detected indirectly. This is an important result since we show that the ^1H chemical shifts for −NH groups in *S. c. ricini* are not resolved in the CRAMPS experiments, thereby preventing their direct measurement. Chemical shifts via dipolar couplings (two-spin and multiple-spin interactions) are also detected for dilute peptides in the silk fibroins, again providing key structure information for these functional residues that is completely absent in the CRAMPS data. Relative dynamics of bulky side groups from dilute amino acid residues are apparent from the 2D multiple-pulse data. Differential spin-diffusion behavior is observed in a modified HETCOR experiment for *S. c. ricini* relative to the *B. mori* protein, suggesting morphological differences in the arrangement of crystalline segments in the proteins. Information regarding hydrogen bonding and constrained interchain spin pairs is provided based on comparison of cross-peak intensities for several nearest-neighbor C−H spin pairs within the chain and based upon the presence of CO correlations with specific α-hydrogens.

Introduction

Structure determination in polypeptides and proteins requires knowledge of local bonding, short-range chain conformation, and long-range geometry or secondary structure. Further, the role of hydrogen bonding in determining secondary structures is a key experimental target in complex protein structure analysis. Solid-state NMR has emerged as an attractive experimental tool in probing chain conformation, hydrogen bonding, and secondary structures in polypeptides, since the native form of the polymer structure may be studied without the complicating effects of dissolution. Recent publications in which NMR has been used to interrogate hydrogen bonding in the solid state have focused on crystalline dipeptides or polypeptides as model systems.[1−4] Others have studied macromolecules in which specific isotopic labels have been introduced to probe the spatial arrangement of monomer pairs, torsion angle distributions, and the dynamics of individual side groups.[5−9] McDermott and co-workers provided a particularly important demonstration of the power of 2D solids NMR to interrogate structure and hydrogen bonding in model peptides at natural abundance.[4] Shoji and co-workers have done extensive multinuclear (^{13}C, ^1H, and ^{15}N) NMR work demonstrating the sensitivity of backbone carbonyl (CO), backbone methylene/methine (CH_2/CH), and amide chemical shifts to local and overall conformation in model polypeptides.[2,3] Recent CRAMPS data suggest that the ^1H chemical shifts of both the α and amide hydrogen are sensitive to secondary α-helix or *β*-sheet structures in homopolypeptides. However, for complex proteins, such chemical shifts may not be resolved even in the CRAMPS experiments. This is particularly true for amide hydrogens. Although some recent work by Shoji and co-workers has demonstrated the utility of multiple pulse 2D methods for the analysis of silk fibroins with regard to backbone H_α shifts, complete structure correlations involving key functional groups (e.g., carbonyl, amide, hydroxyl) were not reported.[10] We report experimental results for two different silk fibroins that illustrate the chemical shift, dipolar coupling, hydrogen bonding, and dynamics information that may be obtained for proteins *at natural abundance* using multiple-pulse 2D techniques.

In this article, we present multiple-pulse ^1H CRAMPS[11,12] and 2D solid-state $^1H-^{13}C$ HETCOR[13−15] data for solid, fibrous proteins obtained from the silk worms *Samia cynthia ricini (S. c. ricini)* and *Bombyx mori (B. mori).* Silk fibroins are fibrous proteins rich in glycine and alanine (ca. 70−80 mol % total), with a primary structure consisting of the repetitive sequence $(Gly\text{-}Ala\text{-}Gly\text{-}Ala\text{-}Gly\text{-}Ser)_n$ in the *B. mori* case, and long polyalanine blocks plus glycine-rich blocks in the *S. c. ricini* protein.[8,16] Each protein contains small amounts of tyrosine (Tyr) and valine (Val), and a secondary structure that is best described as a distorted antiparallel *β*-sheet structure, depending upon whether the fibers exist as the silk I or silk II forms.[7,8] The silk II conformational form was investigated in this study. A key difference between the *S. c. ricini* and *B. mori* fibroins is in the location of the serine residue; serine resides in the less crystalline glycine-rich blocks of the former while it is primarily found in the repetitive, crystalline sequence of the latter. The structures of the primary amino acid residues for the major constituents in silk fibroin are shown in Scheme 1.

The goal of our work on these solid proteins is to determine the level of chemical shift information and dipolar coupling data relevant to structure, hydrogen bonding, and differential dynamics that may be detected at natural abundance using multiple-pulse NMR techniques.

* To whom all correspondence should be addressed.

10.1021/ma012067s CCC: $22.00
Published on Web 02/21/2002

Scheme 1

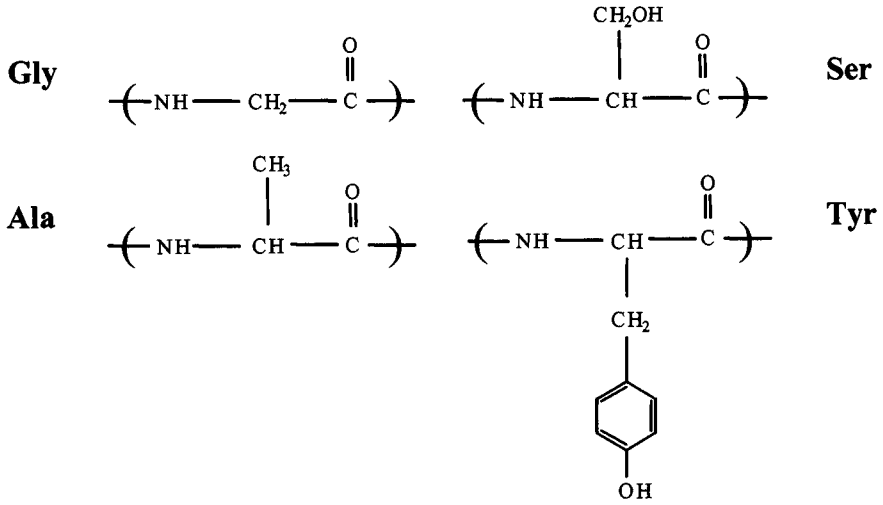

Experimental Section

CRAMPS data were obtained with the MREV-8 sequence on a Bruker DSX-300 instrument using the ^{1}H channel of a 4 mm triple-resonance XY−H magic-angle spinning probe. 90° pulse widths were 2 μs with an interpulse spacing of 2 μs. Spinning speeds were controlled at 1.5−2.0 kHz and were chosen for each sample to minimize spurious rotor lines. The chemical shift scaling factor was experimentally determined to be 0.52 by measuring the offset dependence of a confined H_2O signal. The ^{1}H chemical shift was referenced to poly(dimethylsiloxane) at 0.15 ppm. For each spectrum, 16 scans were acquired with a repetition time of 10 s. The HETCOR experiment of Burum and Bielecki[13] was used for the 2D solid-state heteronuclear correlation results, and 90° pulse widths were 3.2 μs on each channel. Data were collected using one, two, or three windowless isotropic mixing (WIM) cycles. The experimental verification of proper HETCOR performance was done using monoethylfumarate, and carboxylic acid carbon correlations to olefinic and acid protons were observed using both one and two WIM cycles.[15] For longer-range dipolar couplings, controlled periods of ^{1}H−^{1}H spin diffusion were introduced prior to the isotropic ^{1}H/^{13}C polarization transfer step. The chemical shift scaling factor in the ^{1}H dimension was measured experimentally to be 0.42 (near the theoretical 0.47 value), and the proton frequency was shifted off-resonance by 4 kHz from the carrier to avoid any zero-frequency artifacts and take advantage of second averaging effects. Spinning speeds of 3.8−4 kHz were used to minimize potential sideband overlap with peaks of interest. These spinning speed periods (250−290 μs) were larger than twice the WIM cycle length, thereby preventing signal elimination or attenuation due to a refocusing of the C−H dipolar interaction at the end of each rotor period. Typically, 1024 scans were taken for each of 64 points in the t_1 dimension, and recycle delays of 4 s were used. The total experiment time was typically 36 h. Quadrature detection was maintained in the t_1 dimension via use of TPPI. The data were processed with 50 Hz line broadening and zero-filled to 512 points in the t_1 dimension prior to Fourier transformation.

Results and Discussion

CRAMPS Experiments. High-resolution ^{1}H solid-state NMR experiments using CRAMPS (combined rotation and multiple pulse spectroscopy) is a logical choice for characterization of solid-state hydrogen bonding in proteins based on expected perturbations of proton shifts. However, unambiguous assignments would require resolution of "free" and "bound" hydrogens, i.e., those protons that were or were not involved in hydrogen bonding. This is a difficult task given the relatively poor resolution of CRAMPS for macromolecules. The 300 MHz ^{1}H CRAMPS spectrum for *S. c. ricini* and *B. mori* silk fibroins are shown in Figure 1a. Similar to the recent work by Shoji and co-workers,[10] resolved Ala β CH_3 and α CH/CH_2 signals from the Ala and Gly amino acid residues are observed at 1.2 and near 5 ppm, respectively. Since the Gly and Ala residues make up 75% of the protein in each case, the fact that the chemical shifts for H_α's are near 4−5 ppm is consistent with the presence of a β-sheet structure.[2] Broad, poorly resolved signals exist in the region from 6 to 10 ppm. The majority of the intensity in this region may be

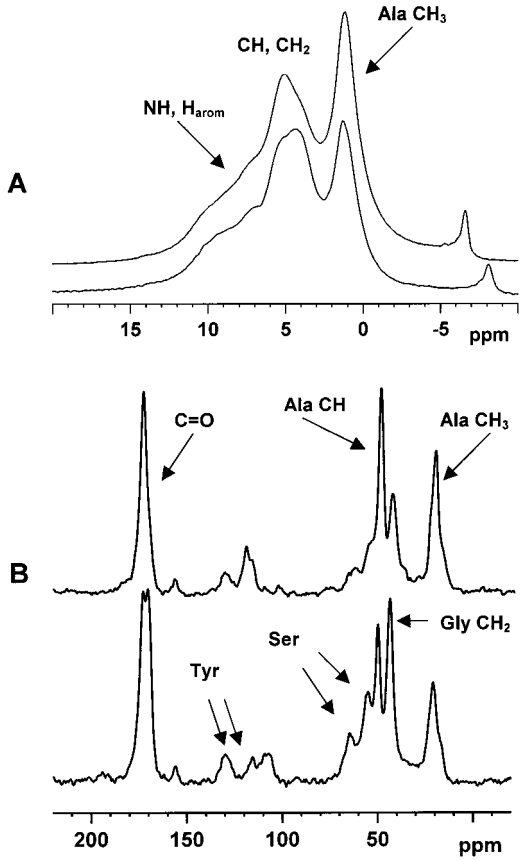

Figure 1. (a) ^{1}H CRAMPS spectra of *S. c. ricini* (top) and *B. mori* (bottom) silk fibroins. (b) ^{13}C CP/MAS spectra of *S. c. ricini* (top) and *B. mori* (bottom) silk fibroins. Peaks are labeled according to the structures presented in Scheme 1.

assigned to the NH hydrogens (as they are present in each repeat unit) as well as a small contribution from aromatic hydrogens in the dilute Tyr (tyrosine) units. While assignment of NH and aromatic shifts via deconvolution might be possible in the *B. mori* case, clearly such shifts are not resolved in the *S. c. ricini* fibers. Amide ^{1}H signals are expected to be broad due to the dipolar coupling between the $I = {}^1/_2$ proton and the quadrupolar ^{14}N nucleus. Further, one might expect that hydrogen bonding both within and between different amino acid segments could lead to inhomogeneous contributions to the line width. The spectral resolution in Figure 1 is not sufficient to identify individual signals from NH groups in any amino acid, much less for backbone hydrogens, aromatic hydrogens, or hydroxyl groups from dilute Ser, Tyr, or Val residues. As such, the available ^{1}H chemical shift information that might be used to follow conformation and hydrogen bonding in different protein structures is limited in the CRAMPS data.

^{13}C CP/MAS spectra are also shown in Figure 1b for reference when viewing the 2D contour plots in subsequent figures.

Isotropic Polarization Transfer HETCOR Results on *S. c. ricini*. Figure 2 shows results from the 2D solid-state HETCOR experiment on the *S. c. ricini* sample. These data were obtained using 1, 2, or 3 WIM cycles (a, b, and c, respectively) for isotropic polarization transfer.[14] The advantage of this experiment is that simultaneous ^{13}C and ^{1}H chemical shift information is obtained along with distance-dependent dipolar coupling data. As such, hydrogen-bonding partners in macromolecules can be identified.[17] Carbon signals are only observed for those carbons with proximate hydrogens (<0.35 nm), as polarization is transferred from each type of hydrogen to nearby carbons in the absence of ^{1}H−^{1}H spin diffusion. The contour plots in Figure 2 and subsequent figures show a relatively large spectral area. To maximize the area available for displaying the 2D data, we have deliberately chosen to leave off the projections along the first and second dimensions. Peaks are labeled appropriately throughout the plots, however. In this way, the correlation spectra may be presented at larger scale in each dimension, thereby allowing better inspection of the data. In Figure 2a, most of the peaks observed in the contour plot arise from carbons with directly bonded hydrogens, e.g., the α CH_2/CH signals from Gly and Ala at 44 and 51 ppm, respectively. Although expected, such peaks are informative, as the conformational dependence of both the ^{13}C and ^{1}H chemical shifts on α-helix or β-sheet structures is obtained in a correlated measurement as previously demonstrated.[10] The ^{1}H chemical shift values for the Gly CH_2 and Ala CH hydrogens may now be clearly detected at 4.3 and 5.1 ppm, respectively. The Ala CH_3 group shows a strong correlation at 21 and 1.2 ppm for the ^{13}C and ^{1}H dimensions. Of much more interest, however, are the correlations arising from the nonprotonated carbonyl carbon at 172 ppm and signals originating from the functionalized Ser and Tyr peptides that are present at relatively low concentrations. Two correlated ^{1}H shifts are detected for the carbonyl carbon: one in which polarization is transferred from protons with a chemical shift of 4.3 ppm and the other from protons with a chemical shift of 8.0 ppm. The former correlation originates from dipolar coupling between CO carbons and α-CH_2 hydrogens, as is easily observed in

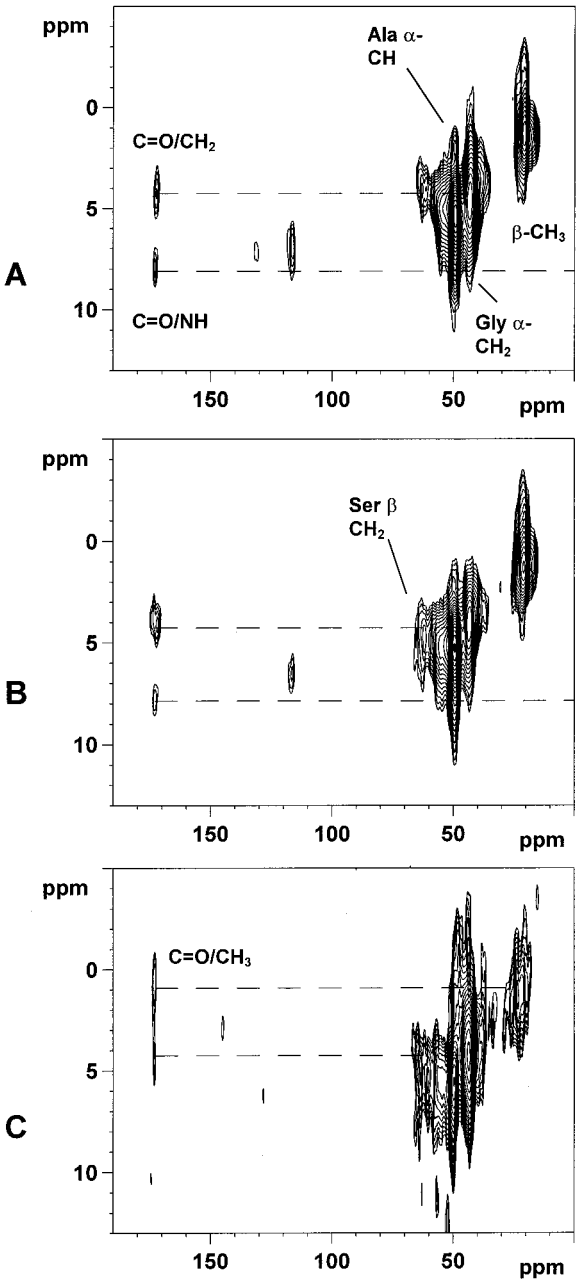

Figure 2. Two-dimensional ^{1}H−^{13}C heteronuclear correlation plots for *S. c. ricini* silk fibroin obtained using (a) one, (b) two, (c) or three windowless isotropic mixing (WIM) cycles. As stated in the text, each contour peak is labeled according to its proton/carbon dipolar correlation, and dashed lines are provided to identify correlations. Clearly, the CO/Gly-CH_2 coupling exists, while the CO/NH coupling does not show correlation with any other carbon peak in the spectrum. While the results for (a) and (b) are similar, the three-WIM cycle data in (c) shows a new CO/Ala-CH_3 coupling.

the contour plot. In the second case, the carbonyl carbons undergo polarization transfer with hydrogens exhibiting a unique, downfield chemical shift at 8.0 ppm. No other carbons display detectable polarization tranfer with these particular protons at 8.0 ppm during the 72 or 144 μs (one or two WIM cycles) mixing time. We assign these relatively strong correlations to the dipolar coupling between carbonyl carbons and the neighboring −NH protons, since each peptide linkage contains this pair. These cross-peaks are well-resolved and allow complete discrimination of the amide-linkage ^{1}H chemical shifts, which could not be assigned from the direct-

observation CRAMPS experiments of *S. c. ricini* in Figure 1a.

With regard to dipolar coupling of the carbonyl carbon to neighboring hydrogens, further information is obtained using three WIM cycles as shown in Figure 2c. Here, in addition to the previously observed correlation to the main-chain hydrogens of Gly residues, a new correlation with the Ala CH_3 (^1H $\delta = 1.2$ ppm) group is observed. Recognizing that attenuation of dipolar interactions involving CH_3 protons occurs due to rapid C_3 rotation, the fact that this CO/CH_3 interaction takes longer to evolve (three WIM cycles) is a combined distance and dynamics effect, and stronger couplings for more rigid "spin pairs" at distances greater than this 0.277 nm distance should be detectable using isotropic mixing (as reported in ref 4 for crystalline amino acids). We note that the calculated distance (using commercial CambridgeSoft Chem3D software on energy-minimized chains of 10 repeat units) between the carbonyl carbon and the CH_3 hydrogens in the same peptide strand is 0.277 nm for a polyalanine model. For comparison, the energy-minimized distances for the interchain CO/NH $^{13}C-^1H$ spin pair in polyalanine is 0.207 nm.

In addition to resolving the chemical shift for the amide protons via the carbonyl carbons, the aromatic ring hydrogens from the Tyr residue are clearly identified at 6.8 ppm via their dipolar correlation with the ring meta carbons at 117 ppm. Further, the ortho and meta hydrogens have different ^1H shifts, as seen by the ortho H−C aromatic correlation at 131 ppm in the ^{13}C dimension. Oddly, the correlation for the ortho position C/H pairs in the ring is significantly weaker than the meta ring pairs and even weak relative to the carbonyl correlations. This anomalous result differs from that observed for the *B. mori* fibroin (vide infra) and will be discussed in more detail below.

A particularly interesting result from the data in Figure 2 may be seen by comparing the correlation behavior of the Ser β (−C**H**$_2$OH) signal at ca. 62 ppm in the ^{13}C dimension as a function of the isotropic polarization transfer time. In Figure 2a, obtained using one WIM cycle, the correlated proton shift is 3.6 ppm, while the much stronger, well-resolved correlation obtained with two WIM cycles exhibits a ^1H shift of ca. 4.6 ppm. Multiple experiments run at different spinning speeds provided identical, reproducible results for this correlation. While this outcome might suggest the presence of two different populations of Ser side groups, it seems unlikely the ^1H chemical shift of the β hydrogens would change by almost 1 ppm, even for hydrogen-bonded vs free Ser side groups, since the β hydrogens are three bonds removed from the hydrogen-bounded hydroxyl proton. We do not have a complete explanation for this behavior at this time. Similar experiments on *B. mori* (vide infra) showed a constant value for the Ser β hydrogen shift, and given that the correlation is so weak in the one WIM experiment of Figure 1a, we take the 4.6 ppm data from Figure 1b as the accurate measure of the Ser β (−C**H**$_2$OH) chemical shift.

Spin-Diffusion HETCOR Results on *S. c. ricini*. Introducing controlled periods of $^1H-^1H$ spin diffusion prior to the WIM polarization transfer step allows longer-range structural features to be identified, and new correlations are detected.[18−20] Parts a and b of Figure 3 show HETCOR results in which 100 and 200 μs of spin diffusion occurred prior to polarization transfer, respectively, for the sample of Figure 2. In 3a, one observes simultaneously the three correlations for the carbonyl group (172 ppm) that were previously detected separately using differing WIM cycles. The third correlation, which was observed using three WIM cycles in Figure 2, corresponds to the Ala-CH_3/CO dipolar coupling. For the first time, we observed multiple yet resolved ^1H correlations for the Ala α-carbon (three total correlations, two of which are new resulting from the spin-diffusion period). These correlations indicate nearest-neighbor dipolar coupling of the α-carbon with the β-methyl protons and the NH protons. Also, the carbons from the β-methyl group exhibit coupling with the NH protons, as evidenced by the weak $^{13}C/^1H$ 21 ppm/8 ppm cross-peak. However, little polarization transfer is observed between Ala and Gly residues, as evidenced by the fact that the Ala α-CH and Gly α-CH_2 ^1H chemical shifts are still unique; i.e., they have not converged to a common value as would occur if spin diffusion had equilibrated the proton spin reservoir from each moiety during the 100 μs time period. However, after 200 μs (Figure 3b), one observes converging chemical shifts for the Ala and Gly α-hydrogens (compare to the same correlations in Figure 2b, for example), as well as a new correlation between the Ala CH3 and the Gly α-CH_2 peaks. Also, ^1H chemical shift resolution for the CO carbon correlations is lost, since all couplings are mixed through spin diffusion.

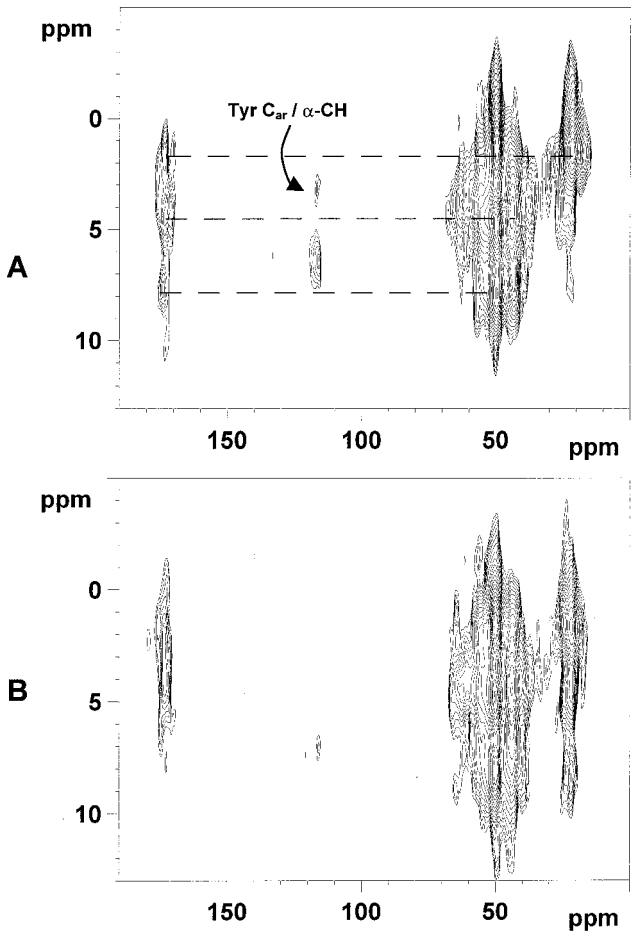

Figure 3. Two-dimensional $^1H-^{13}C$ heteronuclear correlation plots for *S. c. ricini* silk fibroin obtained by inserting (a) 100 μs or (b) 200 μs of $^1H-^1H$ spin-diffusion time prior to the heteronuclear polarization transfer step. In particular, note the multiple correlations for the C═O peak, the Ala-CH peak at 51 ppm, and the Tyr aromatic carbon peak at 117 ppm.

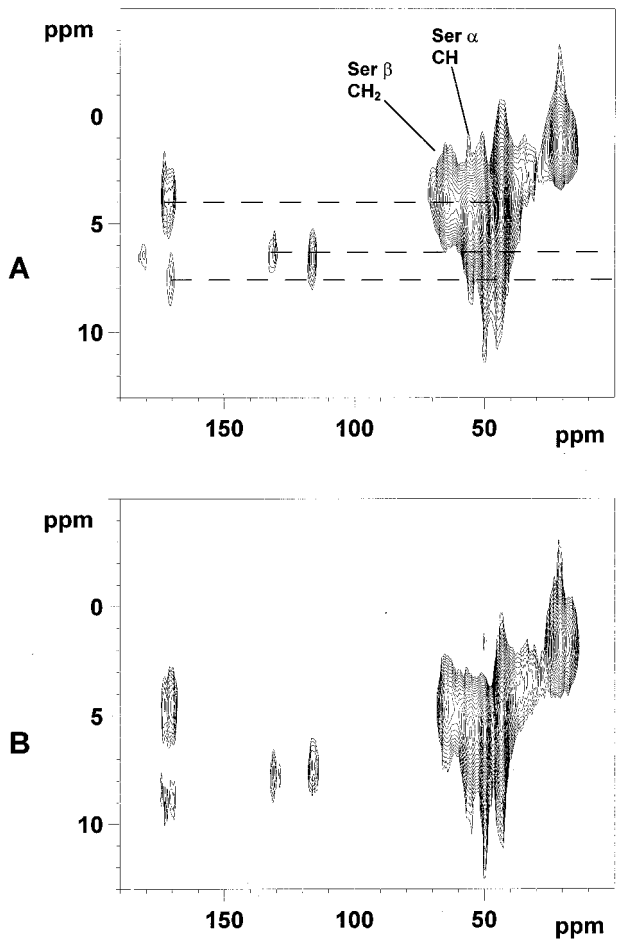

Figure 4. Two-dimensional $^{1}H-^{13}C$ heteronuclear correlation plots for *B. mori* silk fibroin obtained using (a) one or (b) two windowless isotropic mixing (WIM) cycles. Note the significant increase in peak intensity for the Ser and Tyr correlations compared to Figure 2.

In the 100 μs experiment of Figure 3a, a new correlation involving the dilute Tyr meta-aromatic ring carbons is observed that was not previously detected in the absence of spin diffusion. The correlated ^{1}H shift, which is unique and not shared by other (detectable) carbons, is 3.5 ppm. This new correlation may be assigned to the dipolar coupling arising from aromatic ring carbons and β hydrogens in the Tyr residue. We note that the this new ^{1}H chemical shift, detected even in the absence of its own ^{13}C peak, agrees with known ^{1}H solution shifts for Tyr β hydrogens that are reported to range from 3 to 3.5 ppm depending upon solvent.[25]

Isotropic Polarization Transfer HETCOR Results on *B. mori*. 2D correlation results for the *B. mori* silk protein are shown in Figure 4a (one WIM) and 4b (two WIM). As mentioned previously, the amino acid composition and sequence in this silk fibroin are different than in *S. c. ricini*, particularly with regard to the Ser environment. The data in Figure 4a, when compared to that in Figure 2a, are consistent with the different structures. While Ser is present in only slightly larger concentrations in *B. mori*, the α and β carbon correlations are much stronger after only one WIM cycle, comparable in intensity even to the Ala and Gly peaks. This result indicates that the Ser residues occur in a much more rigid, constrained structural unit in the *B. mori* fibroin relative to their environment in *S. c. ricini*, consistent with their placement in the crystalline regions of the former and less-ordered regions of the latter. Different ^{1}H chemical shift values for the Ser-β CH2 group are observed in *B. mori*; one can clearly identify the α and β ^{1}H chemical shifts for the Ser at 4.9 and 3.8 ppm, respectively, via the 56 ppm α and 64.5 ppm β ^{13}C peaks. Recall that the Ser-β CH2 ^{1}H chemical shift was 4.6 ppm in Figure 2b for *S. c. ricini*. This is an important result, since such different chemical shift results could not be detected in any other direct observation experiment for these dilute but structurally important amino acid residues. Unlike the case for *S. c. ricini* in which the apparent Ser β ^{1}H shift changed with increasing number of WIM cycles, the 64.8 ppm/3.8 ppm correlation is constant for the data shown in Figure 4a,b. Also, and again in contrast to the results in Figure 2a,b, strong correlations are observed for both the meta and ortho aromatic ring carbons of Tyr in Figure 4a,b, suggesting a more rigid structure for this side group in *B. mori* since the Tyr concentration is identical in each protein.

Although differences are evident in the dipolar coupling/chemical shift data for the two proteins, key similarities are also apparent. The carbonyl group at 172 ppm in the ^{13}C dimension displays the same two couplings to α-CH_2 and amide-NH protons in the *B. mori* fibroin for either one or two WIM cycles, again allowing clear chemical shift assignment for the NH protons. While different ^{1}H chemical shifts were observed for the Ser β hydrogens relative to *S. c. ricini*, comparison of the Ser α-correlations (56 ppm ^{13}C shift) in Figures 4b and 2b shows identical 4.9 ppm values in each silk fibroin type. The fact that the ^{13}C and ^{1}H chemical shifts are almost identical for the Ser α group in *B. mori* and *S. c. ricini* while they differ by almost 3 ppm (^{13}C) and 1 ppm (^{1}H) for the Ser β moiety suggests that either (1) the β group is more sensitive to the different sequencing in the two cases or (2) different intermolecular geometries involving the polar Ser side group exist. The second possibility is more reasonable, since homopolypeptides have similar shifts as found in mixed peptide proteins for the same conformation, and each of these proteins have β-sheet secondary structures. It was previously shown that the dynamics of the Ser side chain were different in the two proteins, based on the relative magnitude of the C−H dipolar coupling as manifest by the cross-peak intensities in Figure 2 vs Figure 4. It is reasonable, therefore, to associate the observed chemical shift and molecular dynamics behavior with a unique local geometry induced by differing through-space/interresidue hydrogen-bonding interactions of the Ser side chain. The fact that the *B. mori* protein exhibits the most rigid Ser side-chain structure while also showing the most upfield ^{1}H shift value for the β hydrogens is not inconsistent with a more rigid or larger fraction of hydrogen-bonded groups relative to *S. c. ricini*. These conclusions are consistent with the fact that most of the Ser residues are located in the crystalline repeat sequence of *B. mori*, a regular sequence which is no doubt stabilized by secondary hydrogen-bonded structures.

Spin-Diffusion HETCOR Results on *B. mori*. HETCOR experiments with 100 and 200 μs of spin-diffusion were completed. Since the results are very similar to those for *S. c. ricini* in Figure 3, the figures are not shown for brevity. As in Figure 3, multiple correlations are observed for the CO, α-CH/CH_2, and β-CH_3 peaks. Minor differences include the development

of a clearly resolved NH/α-CH_2 cross-peak for Gly after 200 μs, which was not observed in Figure 3. Also, the Ala and Gly α-hydrogen chemical shifts are completely converged to the same value after 100 μs of spin diffusion, while in the *S. c. ricini* experiment, this was not complete even after 200 μs. While more detailed spin-diffusion experiments would be necessary to elucidate the average separation distance of the Ala-rich and Gly-rich repeat blocks in the *S. c. ricini* fibroin (by measuring the time evolution of ^{1}H slices through the Gly α-CH_2 and Ala β-CH_3 peaks), the more rapid convergence observed for *B. mori* is consistent with the repeat sequence of (-Ala-Gly-) residues in the crystalline regions.

Implications of Results on Hydrogen Bonding. An optimum outcome from these experiments would be to unambiguously identify hydrogen-bonding pairs, i.e., donors and acceptors, which induce secondary structure. Unfortunately, hydrogen bonding involving intraresidue or nearest-neighbor spins within the chain leads to the same type of HETCOR response as interchain hydrogen bonding, since each chain has the same amino acid composition. However, some key evidence for hydrogen bonding between adjacent peptide strands in the β-sheet structure is provided in the experimental results. The through-space intrachain C−H distances for CO/NH vs α-CH/NH or α-CH_2/NH groups are all within 0.05 Å of one another, and yet after one or two WIM mixing cycles, only CO/NH correlations are observed (Figures 2 and 4). In fact, correlations between the amide NH hydrogen and Ala α-CH or Gly α-CH_2 carbons are not observed until at least 100 μs of spin diffusion occurs (Figures 3 and 5). Since each of these functional groups (CO, NH, CH, CH_2) are nearest neighbors within the chain and, as stated previously, have similar internuclear distances with the NH hydrogen, their polarization transfer dynamics and therefore cross-peak intensities should be similar for a given experiment (assuming no large difference in conformational dynamics along the chain). In other words, if the detected CO/NH polarization transfer resulted *only* from intraresidue dipolar coupling, then the correlation would be expected to be very weak or nonexistent based on the lack of these other intraresidue couplings with the NH proton under isotropic mixing conditions. We believe that the much stronger CO/NH correlation observed in both silk fibroin types is due to hydrogen bonding between peptide strands on neighboring β-sheets, which acts to constrain the C−H dipolar pair arising from the CO group on one chain and the NH group on the adjacent chain. In this way, the relative dipolar coupling constant is enhanced *for that spin pair* compared to an adjacent carbon spin within the same chain at a similar internuclear distance from the amide hydrogen.

Supporting evidence for this suggestion of constrained spin pairs between chains comes from a more detailed examination of the other CO correlation in Figures 2 and 4, i.e., the cross-peak with the Gly α-CH_2 protons at 4.2 ppm in the ^{1}H dimension. In both the *S. c. ricini* and *B. mori* proteins, intraresidue carbonyl/main-chain dipolar couplings were only observed for Gly CH_2 hydrogens in the HETCOR data; no CO/Ala α-CH cross-peaks are observed using 1, 2, or 3 WIM cycles. This was the case independent of the mixing time and spinning speed. Again, CO/Ala α-CH correlations were only observed after introducing a spin-diffusion mixing period (Figures 3 and 5). The absence of the expected CO/Ala-CH coupling in all of the experimental results is puzzling, since the relevant C−H distance between the two groups is 0.215 nm, identical to that for the CO/Gly-CH_2 spin pair. Recently, the idea that interchain α-CH- - -O═C hydrogen bonds are significant and influence structure, particularly in β-sheet proteins, has received much attention. Dixon, Hay, and co-workers suggested, on the basis of computational and crystal structure data, that the strength of these hydrogen bonds is approximately one-half that of the NH- - -O═C bonds—sufficiently strong to influence overall secondary structure.[21] Our HETCOR data in which the CO/Gly α-CH_2 correlation is observed while the CO/Ala α-CH correlation is absent is consistent with the physical picture of interchain hydrogen bonds of this second type, since the α-hydrogens in Gly are more acidic than those in Ala. In Ala, the inductive effect from the attached −CH_3 group reduces the acidity, thereby decreasing the possibility of forming hydrogen bonds with adjacent carbonyl groups. Further, the steric barriers from the attached methyl group in Ala may also preclude interchain bonding. The physical picture that we believe is supported by the HETCOR data is consistent with a recent model proposed by Dixon and Hay for β-sheet structures, in which a single carbonyl group on one peptide chain is "doubly" hydrogen-bonded to amide hydrogens and α-CH_2 hydrogens on a neighboring chain. Again, we base this assignment on the presence of specific couplings involving CO groups as well as on the absence of key couplings that should arise if only intraresidue structure was being probed in the HETCOR experiments. Previous studies on crystalline dipeptides and amorphous synthetic polymers have clearly shown that hydrogen-bonded spin pairs are well within the distance range detected by the isotropic WIM mixing cycle used in the HETCOR experiment.[4,17]

The absence of expected correlations has been discussed previously by McDermott and co-workers for their model peptide experiments, and citing previous work by Griffin, they suggested that this may be due to molecular motions on the same time scale as the multiple-pulse polarization transfer cycle time.[22] The phenomenon of incoherent molecular motion interfering with coherent averaging in NMR is well-known and particularly prevalent in macromolecules. It has been discussed by many authors for a variety of systems.[20,23,24] We addressed this experimentally with regard to the CO/Ala-CH case by varying the spinning speed in the experiment from 3000 to 4500 Hz; the results were similar. A more appropriate experiment would be to vary the WIM cycle length by changing the pulse widths. For the data reported here, pulse widths of 3.2 μs were used for the windowless sequence, corresponding to an effective cycle time of 76.8 μs. Therefore, molecular motions on a time scale of 10−15 kHz could confound polarization transfer. To address this, we performed a separate set of experiments on the *S. c. ricini* in which the pulse width was reduced to 1.65 μs, thereby reducing the cycle time by almost a factor of 2. *Identical results were obtained in terms of not observing any detectable CO/Ala-CH correlations using one or two WIM cycles with the reduced cycle time.* The confounding effects of molecular motion, e.g., conformational librations, around the Ala α-CH group cannot be definitively excluded as the reason why the expected CO correlation is not observed without spin diffusion. Even so, the presence of such motions would not be inconsis-

tent with the physical picture described in the preceding paragraph, since interchain hydrogen bonding acts to constrain the CO and NH groups on either side of the Ala-CH moiety, while still allowing small-amplitude torsional dynamics about the $CO-CH_\alpha$ and $CH_\alpha-NH$ bonds of the Ala residue.

Conclusions

In this contribution, we have shown that important ^1H chemical shift information for amide (NH) hydrogens and dilute but structurally important amino acid residues may be obtained using the 2D HETCOR strategy on solid, natural abundance silk fibroin proteins. By comparing isotropic two-spin polarization transfer data to multiple-spin spin-diffusion results, both ^{13}C and ^1H chemical shift data were obtained for the Tyr residue which was not visible from direct one-dimensional experiments on either nuclei. Differential dynamics of Ser residues in *S. c. ricini* fibroin vs *B. mori* were detected on the basis of heteronuclear polarization transfer dynamics; Ser residues exist in a more rigid or constrained environment in the latter. These conclusions were consistent with the ca. 1 ppm chemical shift difference observed for the Ser β $-CH_2$ group in both the ^1H and ^{13}C dimensions. While direct extraction of hydrogen-bonded spin pairs between peptide strands vs those within peptide strands is not unambiguous from the data, detailed comparisons of CO/NH, CO/α-hydrogen, and NH/α-hydrogen cross-peak intensities indicate that interchain hydrogen bonding clearly contributes to the measured signals. In particular, the recent theoretical model discussed by Dixon, Hay, and co-workers in which *both* CO/NH and CO/Gly α-CH_2 groups stabilize the β-sheet structure through interchain hydrogen bonding is supported by our experimental results.

Acknowledgment. The authors are grateful to Professor Tetsuo Asakura for providing the *S. c. ricini* and *B. mori* silk fibroin samples. Support from the National Science Foundation (DMR-0137968) is gratefully acknowledged.

References and Notes

(1) Lee, D.; Ramamoorthy, A. *J. Phys. Chem. B* **1999**, *103*, 271.
(2) Shoji, A.; Kimura, H.; Ozaki, T.; Sugisawa, H.; Deguchi, K. *J. Am. Chem. Soc.* **1996**, *118*, 7604.
(3) Kimura, H.; Shoji, A.; Sugisawa, H.; Deguchi, K.; Naito, A.; Saito, H. *Macromolecules* **2000**, *33*, 6627.
(4) Gu, Z.; Ridenour, C. F.; Bronniman, C. E.; Iwashita, T.; McDermott, A. *J. Am. Chem. Soc.* **1996**, *118*, 822.
(5) Kummerlen, J.; van Beek, J. D.; Vollrath, F.; Meier, B. H. *Macromolecules* **1996**, *29*, 2920.
(6) Demura, M.; Minami, M.; Asakura, T.; Cross, T. A. *J. Am. Chem. Soc.* **1998**, *120*, 1300.
(7) Asakura, T.; Ito, T.; Okudaira, M.; Kameda, T. *Macromolecules* **1999**, *32*, 4940.
(8) Kameda, T.; Ohkawa, Y.; Yoshizawa, K.; Naito, J.; Ulrich, A. S.; Asakura, T. *Macromolecules* **1999**, *32*, 7166.
(9) Asakura, T.; Nakazawa, Y.; Ghi, P. Y.; Ashida, J.; Kameda, T. *Polym. Mater. Sci. Eng.* **2000**, *86*, 145.
(10) Kimura, H.; Kishi, S.; Shoji, A.; Sugisawa, H.; Deguchi, K. *Macromolecules* **2000**, *33*, 9682.
(11) Burum, D. P.; Bielecki, A. *J. Magn. Reson.* **1991**, *94*, 645.
(12) Gerstein, B. C.; Pembleton, R. G.; Wilson, R. C.; Ryan, L. M. *J. Chem. Phys.* **1977**, *66*, 361.
(13) Bronniman, C. E.; Hawkins, B.; Zhang, M.; Maciel, G. E. *Anal. Chem.* **1988**, *60*, 1743.
(14) Caravatti, P.; Braunschweiler, L.; Ernst, R. R. *Chem. Phys. Lett.* **1982**, *89*, 363.
(15) Bronniman, C. E.; Ridenour, C. F.; Kinney, D. R.; Maciel, G. E. *J. Magn. Reson.* **1992**, *97*, 522.
(16) Mita, K.; Ichimura, S.; James, T. C. *J. Mol. Evol.* **1994**, *38*, 583.
(17) White, J. L.; Mirau, P. A. *Macromolecules* **1994**, *27*, 1648.
(18) Kaplan, S. *Macromolecules* **1993**, *26*, 1060.
(19) Li, S.; Rice, D. M.; Karasz, F. E. *Macromolecules* **1994**, *27*, 2211.
(20) White, J. L.; Dias, A. J.; Ashbaugh, J. R. *Macromolecules* **1998**, *31*, 1880.
(21) Vargas, R.; Garza, J.; Dixon, D.; Hay, B. P. *J. Am. Chem. Soc.* **2000**, *122*, 4750.
(22) Rothwell, W. P.; Waugh, J. S. *J. Chem. Phys.* **1981**, *74*, 2721.
(23) Long, J. R.; Sun, B. Q.; Bowen, A.; Griffin, R. G. *J. Am. Chem. Soc.* **1994**, *116*, 11950.
(24) White, J. L.; Brant, P. *Macromolecules* **1998**, *31*, 5424.
(25) Wishart, D. S.; Sykes, B. D. In *Methods Enzymol.* **1994**, *239*, Chapter 12, 363−392.

MA012067S